Temperature dependence of magnetic anisotropy in a cylindrical $Fe_{65}Pd_{35}$ nanowire array

M. Soledad Aprea[1,2], Julieta S. Riva[1,3], Paula G. Bercoff [*1,2], Manuel Vázquez[4]

[1] Universidad Nacional de Córdoba. Facultad de Matemática, Astronomía, Física y Computación. Córdoba, Argentina.
[2] CONICET, Instituto de Física Enrique Gaviola (IFEG). Córdoba, Argentina.
[3] CONICET, Instituto de Físico Química de Córdoba (INFIQC). Córdoba, Argentina.
[4]Instituto de Ciencia de Materiales de Madrid, CSIC. 28049 Madrid, Spain

Abstract

$Fe_{65}Pd_{35}$ cylindrical nanowires (NWs) were synthesized in commercial anodic alumina porous templates *via* potentiostatic electrodeposition. The morphology, composition, and crystalline structure were analyzed by scanning and transmission electron microscopy, energy-dispersive X-ray spectroscopy, and X-ray diffraction. The NWs obtained are (10 ± 2) μm long and (200 ± 20) nm in diameter, with a polycrystalline microstructure. Magnetic properties were investigated by measuring the Zero Field Cooling-Field Cooling magnetization curves and hysteresis loops in the temperature range 10 K to 350 K. The magnetization easy axis is determined to be along the NWs axis, indicating strong anisotropy in this direction, which cannot be accounted for by only considering shape anisotropy. The hysteresis loops were fitted using the law of approach to saturation, obtaining the effective anisotropy field H_A and the effective anisotropy constant K_{eff} value for different temperatures. The blocking temperature T_B dependence on the magnetic field H was also analyzed, indicating that a blocked magnetic contribution is present, arising from the smaller grains in the NWs. The observed enhancement in the effective magnetic anisotropy of the array throughout the studied temperature range is explained by considering magnetic interactions among these nanograins.

Keywords: Nanowire array, effective anisotropy, Fe-Pd alloy; cylindrical nanowires

1. Introduction

Magnetic nanostructures containing magnetic noble metals have been the subject of intense research motivated not only by these materials interesting properties ─quite different from those of their bulk counterparts─ but also because of their promising technological applications, such as magnetic recording media, ferrofluids, soft and hard magnetic materials, physico-chemical, biomedicals, catalysis or sensors [1-4]. This type of nanostructures can be adapted to improve their performance by controlling their size, shape, composition, and surface properties [5]. On the other hand, one-dimensional nanostructures such as magnetic nanowires, rods, and nanotubes, are very interesting due to their large shape anisotropy which can enhance the magnetic properties [6]. Particularly, cylindrical magnetic nanowires (NWs) are a promising example of building blocks of 3D nanoarchitectures and nanotechnologies [7-11].
Arrays of cylindrical NWs offer new perspectives in which some of the most relevant properties are determined by the magnetism of the individual NWs, while interwire magnetostatic interactions also play a significant role [12]. Besides, NWs are interesting materials for electro-catalysis, due to the advantageous features arising from their shape anisotropy on the electrochemical processes at the electrodes [13]. Also, NWs are employed in heterogeneous catalysis [14] in view of their higher active surface area compared to nanoparticles, and because magnetic catalysts have the advantage of being easily recovered and reused many times avoiding filtration or centrifugation processes [15].
Concerning noble/transition metal alloys, Fe-Pd alloys present very interesting properties that depend on their chemical composition, leading to different magnetic behaviors [16-19]. Particularly, materials with a $Fe_{70}Pd_{30}$ composition present an interesting phenomenon, such as the phase transformation from the austenite cubic phase to the martensite tetragonal phase, which is the basis for the magnetic shape-memory effect [20]. Also, the $Fe_{70}Pd_{30}$ system is a biocompatible and promising material for biomedical applications [21,22]. Furthermore, palladium-rich Fe-Pd alloys have been successfully employed in different catalytic reactions [23], exhibiting a high hydrogen absorption kinetics [24].

In this work we investigate the temperature dependence of magnetic properties of an array of highly ordered $Fe_{65}Pd_{35}$ NWs synthesized by electrodeposition into porous anodic aluminum oxide (AAO) templates. The crystalline structure was verified by X-ray diffraction (XRD), the chemical composition was characterized by energy-dispersive X-ray spectroscopy (EDS), and the morphology was determined by scanning and transmission electron microscopy (SEM and TEM), which evidenced the NWs polycrystalline microstructure. Particularly, the temperature dependence of the magnetic properties, such as coercivity (H_C) and saturation magnetization (M_s), were analyzed. We applied the well-known law of approach to saturation (LATS) [25] for studying the magnetic anisotropy in nanometric materials. This allowed us to obtain the effective anisotropy constant K_{eff} as a function of temperature from the measured magnetization curves for our NW array. This technique has been widely used to determine K_{eff}, M_s, or volumes of interacting particles in different materials, such as Fe nanoparticles [25], $NiFe_2O_4$ [26], Co [27], Fe_3Se_4 [28], amorphous alloy ribbons [29] and MnZn ferrites [30], while it has been seldom applied to study the magnetic behavior of magnetic NWs arrays.

We have also studied the effect of the external magnetic field on the blocking temperature T_B distribution, obtained from the derivative of the Zero Field Cooling - Field Cooling (M_{ZFC} - M_{FC}) magnetization curves. We have analyzed the $T_B(H)$ dependence considering an analogy with a particulate system and using a simple modification of the random anisotropy model (RAM) developed by Nunes et al. for magnetic nanoparticle clusters [31]. The model takes into account the size of the nanoparticles (e.g., nanocrystallites) as well as the field dependence of the correlation length. The value of K_{eff} obtained by LATS was used in the modified RAM to obtain an average nano-grain diameter (D_{av}), and the intergrain exchange constant, A_{eff}. These results are consistent with a magnetic contribution from the smallest crystals in the NWs which are coupled up to second nearest neighbors and which are blocked below room temperature.

2. Materials and Methods

$Fe_{65}Pd_{35}$ NWs were synthesized using commercial anodized alumina oxide (AAO) membranes as templates, provided by Whatman Co. The membranes are 60 μm-thick, with 200 nm nominal pore size diameter and a center-to-center distance of 370 nm, which determine a porosity of $P = 0.26$. Prior to use, a conductive thin gold layer was sputtered on one side of the porous membrane to be used as a cathode. The electrodeposition was carried out at a constant potential of -1.5 V for 30 minutes at room temperature using a potentiostat/galvanostat Autolab and a conventional cell with three electrodes, with a commercial Ag/AgCl electrode as a reference, and a Pt wire as a counter electrode. The solution for the electrodeposition contained 0.1M $FeCl_3$ + 0.04M $PdCl_2$ + 0.3M $C_6H_8O_7$ and 0.25M NH_4OH in ultrapure water.

A Sigma Zeiss Field Emission Scanning Electron Microscope (FE-SEM), with an Oxford Energy Dispersive Spectrometer (EDS) was used to determine the samples' morphology and chemical composition. For these determinations, the AAO template was dissolved with 1.0 M NaOH, and the free NWs were washed several times with distilled water.

The crystalline structures were determined by X-ray diffraction (XRD) in a PANalytical Empyrean diffractometer using Cu Kα radiation (λ= 1.5418 Å) in the 2θ range from 30º to 90º and the patterns were refined with the Rietveld method.

Magnetic measurements were performed in a *Cryogenic* vibrating sample magnetometer, under a maximum field of ± 3 T in the temperature range from 10 K to 350 K applied parallel (PA) and perpendicular (PE) to the NWs axis. The coercive field H_C and the saturation magnetization M_s were obtained from the hysteresis loops after subtracting a linear contribution, arising from the diamagnetic alumina template (Al_2O_3).

3. Results and Discussion

Figure 1(a-b) shows SEM images of $Fe_{65}Pd_{35}$ NWs after completely dissolving the AAO template. Several SEM images let estimate the NWs diameter of (200 ± 20) nm, the same as the pore diameter of the alumina template, and a NWs length of (10 ± 2) μm. The chemical composition of the NWs was determined by EDS and confirms the presence of Fe and Pd, with an atomic proportion of $Fe_{(65\pm5)}Pd_{(35\pm5)}$ and no impurities. The granular structure of the NWs can be clearly seen in the SEM image of Figure 1b, which is also confirmed by bright-field TEM images (Figure 1c) from which a mean grain size D_{TEM} = (5 ± 1) nm is determined.

The crystalline structure of the as-electrodeposited $Fe_{65}Pd_{35}$ NWs was studied by XRD and the corresponding diffractogram with the best fitting obtained by applying the Rietveld refinement are shown in Figure 2. As it can be seen, there is a coexistence of two Fe-Pd alloy phases: *fcc* and *bcc*. The peaks observed around 2θ = 41°, 47° and 68° are associated with the family of planes (111), (002),

(022) of a γ-Fe-Pd disordered *fcc* structure, and the peak close to 2θ = 43° corresponds to the plane (011) of the Fe-Pd disordered *bcc* structure [32].

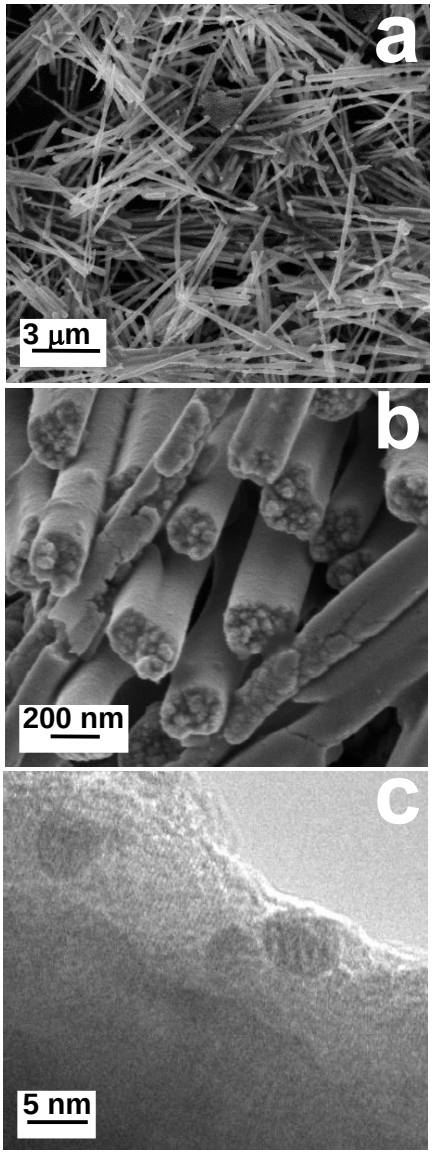

Figure 1: (a, b) SEM images of $Fe_{65}Pd_{35}$ NWs after being released from the AAO template at different magnifications. (c) TEM image of a $Fe_{65}Pd_{35}$ NW.

The amorphous structure of the AAO template originates a large bump in the pattern in the 2θ range 55º to 65º [33,34]. The amount of each phase could be determined from the Rietveld refinement, being 81.5% and 18.5% for *fcc* and *bcc* Fe-Pd phases, respectively. The cell parameters are a_{FePd}^{fcc} = (3.857 ± 0.005) Å for the *fcc* structure and a_{FePd}^{bcc} = (2.937 ± 0.004) Å for the *bcc* structure. The average crystallite size calculated with the Scherrer formula is D_{SCH} = (6 ± 4) nm.

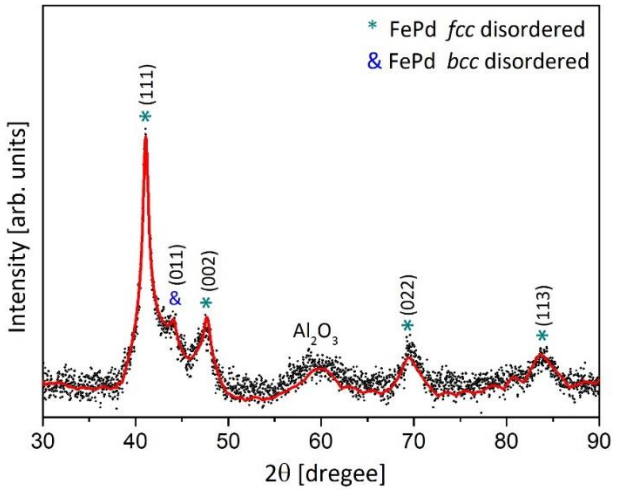

Figure 2: X-ray diffractogram of as-deposited $Fe_{65}Pd_{35}$ NW array within the AAO template. The solid red line is the fit obtained after Rietveld refinement.

Obtaining the thermodynamically stable *fcc* Fe-Pd phase in the as-prepared sample is a remarkable result, since this crystalline structure is the basis for the magnetic-shape-memory effect [34]. The same coexistence of *fcc* and *bcc* phases was previously found in $Fe_{73}Pd_{27}$ ribbons after annealing at 773 K [35]. Specifically, in the case of NWs, a similar XRD pattern was observed for $Fe_{50}Pd_{50}$ NWs inside the AAO template, but only after annealing the sample at 873 K during 120 min [36].

The room temperature magnetic hysteresis loops corresponding to $Fe_{65}Pd_{35}$ NWs inside the AAO template are depicted in Figure 3. The normalized magnetization M/M_s (where M_s is the saturation magnetization) was measured with the applied magnetic field parallel (PA) and perpendicular (PE) to the NWs axis. As it can be deduced, $Fe_{65}Pd_{35}$ NWs display a relatively soft ferromagnetic behavior, with coercivity values of (14 ± 1) mT and (8 ± 1) mT for PA and PE configurations, respectively. When the magnetic field is applied in the PA direction, saturation is achieved at lower saturation fields H_s than in PE configuration. In addition, a larger squareness (M_r/M_s, where M_r is the remanent magnetization) was observed in the PA direction. This observation is consistent with a magnetic easy axis parallel to the NWs axis, which is usually the preferred direction in one-dimensional nanostructures with strong shape anisotropy [37, 38]. Note the high value of the NWs aspect ratio, length/diameter ≈ 10,000 nm/ 200 nm= 50. It should also be noted that despite a marked shape anisotropy is observed, the remanence in the PA hysteresis loop is rather low (M_r/M_s<0.20), indicating that magnetostatic interactions among the NWs are important. This effect has also been reported

for Ni NW arrays in templates with the same porosity as ours [39].
Since the *bcc* and *fcc* cubic phases have a relatively weak magnetocrystalline anisotropy, the shape anisotropy and the magnetostatic interactions among NWs mostly determine the overall magnetic response [40,41].

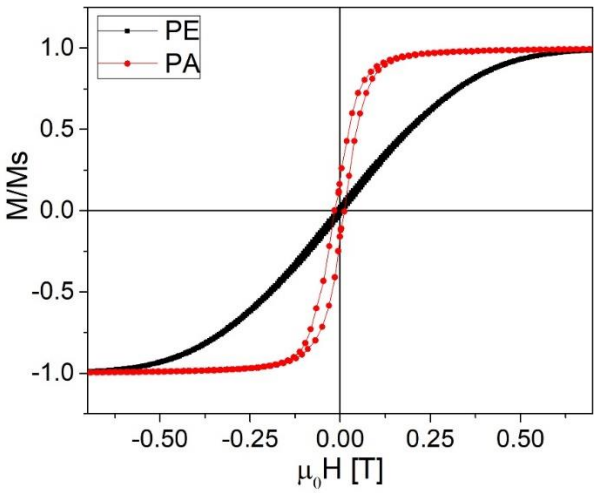

Figure 3: Room temperature magnetic hysteresis loops measured with the applied magnetic field parallel (PA) and perpendicular (PE) to the NWs axis.

In magnetic NW arrays, different contributions to the effective anisotropy constant K_{eff} must be considered (e.g., shape, magnetocrystalline, magnetoelastic and magnetostatic interactions) depending on the particular system [12]. Several methods allow obtaining an estimate of K_{eff} in a NW array. The difference of the saturation fields H_S in the PE and PA hysteresis loops gives a rough estimate of the anisotropy field $H_A=H_S^{PE}-H_S^{PA}$ [42-44] through which the value of the effective anisotropy constant K_{eff} can be obtained using the well-known expression [45]:

$$H_A = \frac{2K_{eff}}{M_S}. \qquad (1)$$

However, for real systems a more accurate method to determine H_A is calculating the difference between the areas enclosed by the demagnetizing branches of the PA and PE hysteresis loops in the first quadrant [44, 45]. Other methods, such as torque magnetometry [46], ferromagnetic resonance[12, 47], experimental determinations involving effective demagnetizing factors [48] or the Law to Approach to Saturation (LATS [25], described in detail below) can also be used to evaluate K_{eff} in NW arrays.

In order to determine K_{eff} from Eq. 1, H_A and M_s are needed. Using the area method described above and the data of Figure 3, H_A = 0.33 T was obtained. Because the absolute magnetization value for a NW array can be experimentally determined only with significant error, unless a more precise technique such as ferromagnetic resonance is available, in this work relative values of magnetization are presented. Therefore, in Eq. 1 the value M_s=1.474 x 10^6 A/m from Fe-Pd polycrystalline alloy measurements by Recarte et al. [49] was considered. This gives K_{eff}=2.4 x 10^5 J/m^3 for our sample at room temperature. Note that the shape anisotropy energy density for Fe NW arrays (12 nm diameter, 10 μm long) was reported to be 9.5 x 10^5 J/m^3 while the magnetocrystalline anisotropy constant was just 0.45 x 10^5 J/m^3 [50], indicating that in NWs of large aspect ratio and cubic crystalline structures, in which the magnetocrystalline anisotropy is relatively small, the effective anisotropy is mostly determined by the shape anisotropy. In the particular case of an austenitic (*fcc*) $Fe_{70}Pd_{30}$ single crystal, it is found that the magnetocrystalline anisotropy constant is K_1=-0.046 x 10^5 J/m^3 at room temperature [51]. This is by far very small to account for the estimated K_{eff} value, which is thus considered to arise from the shape anisotropy coming from large aspect ratio NWs and other contributions to the effective anisotropy (e.g., magnetoelastic and/or magnetostatic interactions from the NWs [52, 53]). In the following we present a further investigation on this matter, involving temperature-dependent measurements.

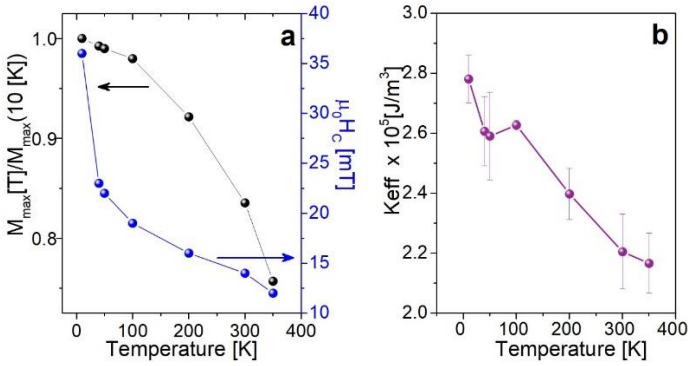

Figure 4: (a) Temperature dependence of M_{max}(T) /M_{max}(10 K) and H_c for the NW array investigated at PA configuration. (b) K_{eff} values at different temperatures were obtained using the *LATS* method.

The magnetic hysteresis loops of the $Fe_{65}Pd_{35}$ NW array were measured at different temperatures in PA orientation, with a maximum applied field of 3 T. Figure 4a shows the temperature dependence of the relative maximum magnetization at 3 T M_{max}/M_{max}(10 K) and the coercive field H_c.

Both, coercivity and magnetization, diminish with increasing temperature, however H_c displays a faster decrease at low temperatures. This may indicate the presence of additional mechanisms that contribute to lower the effective anisotropy, since if shape anisotropy were dominant in the whole temperature range, the overall behavior of coercivity and magnetization should be similar. However, following the analysis by Bran et al. for Co-Fe NW arrays [40], we infer that shape anisotropy might dominate in our system, since dHc/dT is always negative. On the other hand, if only shape anisotropy were the responsible for the observed K_{eff} decrease with T in the whole temperature range (roughly 30% between low and high temperature, as shown in Figure 4a) a ~50% decrease in K_{eff} should be observed since $K_{shape} \sim M_s^2$. However, a decrease of about 20% instead of the expected 50% is observed in the same temperature range (Figure 4b). We further investigate this enhancement of the effective anisotropy below.

The Law of Approach to Magnetic Saturation (LATS), which describes the dependence of magnetization M_H with the applied field for $H >> H_C$, is an effective method to determine magnetic anisotropy in magnetic materials [49, 54, 55]. In order to obtain more information about the magnetic characteristics of the Fe-Pd NW array, we used the relative $M_S(T)/M_S(T=10\ K)$ values shown in Figure 4a and applied the general expression of the LATS given by Kronmüller et al. [56]:

$$M_H = M_S(T)\left(1 - \frac{a}{H} - \frac{B}{H^2} - \cdots\right) + \chi_P H \quad (2)$$

where M_H is the magnetization (along the field direction) in the field H, M_s is the saturation magnetization and a and B are parameters that characterize the sample. We discard the paramagnetic term $\chi_P H$ since it only becomes relevant at applied fields much higher than the ones used in this work. The a/H term is attributed to the existence of local inhomogeneities and defects in the material, where the parameter a is proportional to the relevance of such inhomogeneities [55]. The term B/H^2 is related to the macroscopic magnetic anisotropy, including the magnetocrystalline, the shape, and the magnetoelastic anisotropy terms. The parameter B is proportional to the effective anisotropy constant K_{eff}, and can be expressed as [25]:

$$B = \frac{4}{15}\left(\frac{K_{eff}(T)}{M_S(T)}\right)^2 . \quad (3)$$

The high-field portions of the magnetization curves obtained at different temperatures were fitted with Eq. 2, obtaining B from the fitting parameters.

Using this result, the values of K_{eff} at different temperatures were calculated from Eq. 3, and are shown in Figure 4b. The maximum values of K_{eff} are between 2.8 x 10^5 J/m^3 and 2.6 x 10^5 J/m^3 at T < 100 K, and the minimum value is around 2.2 x 10^5 J/m^3 at 350 K. It is worth mentioning that with this method, K_{eff} is 2.2 x 10^5 J/m^3 at 300 K, close to the value calculated from the anisotropy field H_A taken from the room temperature hysteresis loops in PA and PE configurations and Eq. (1).

Magnetization vs. temperature curves were measured between 5 K and 300 K in PA configuration, following the Zero Field Cooling-Field Cooling (ZFC-FC) protocol with an applied magnetic field of 10 mT.

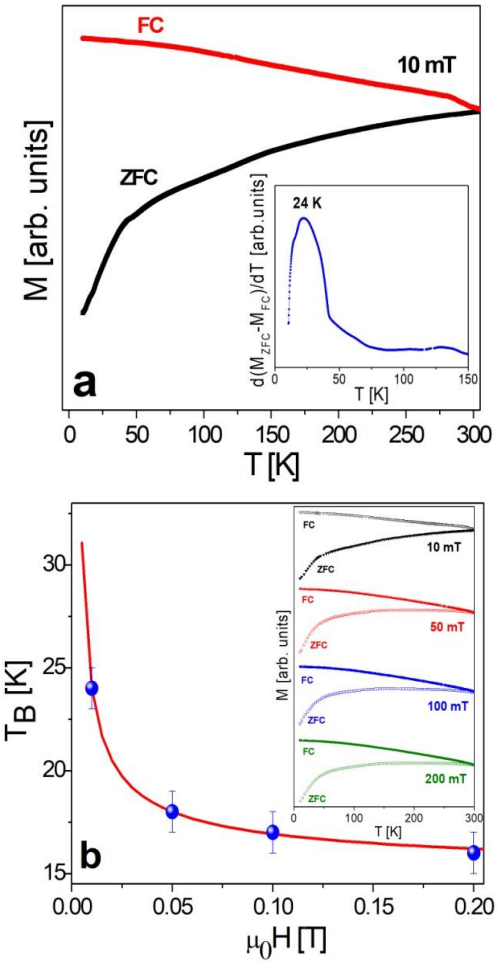

Figure 5: (a) ZFC-FC curves of the $Fe_{65}Pd_{35}$ NW array with an applied field of 10 mT. Inset: Blocking temperature distribution $\partial[M_{ZFC}\text{-}M_{FC}]/\partial T$. (b) Blocking temperature as a function of applied field $T_B(H)$. The red solid line is the best fit of Eq. (6) to the experimental data. Inset: ZFC-FC curves measured at different applied fields.

Figure 5a depicts the ZFC-FC curves which show that the irreversibility temperature (the merging point of the ZFC and FC curves) is above 300 K indicating a strongly interacting system, as may be expected for the NW array with P=0.26. Deriving the difference between the M_{ZFC} and M_{FC} magnetization curves ($\partial[M_{ZFC}\text{-}M_{FC}]/\partial T$) gives the profile of the blocking temperature T_B distribution, which is related to the energy barrier distribution in the sample. From this curve, the mean T_B can be easily estimated as the maximum [31]. The inset in Figure 5a shows that a clear peak at T_B = 24 K appears, indicating that there is a magnetic contribution which is blocked below 24 K. In our NW array this contribution may arise from the smaller crystallites in the NWs which can be considered as activation or Barkhausen volumes [57]. Thermal fluctuations influence the hysteretic behavior of the system since they may lead to overcoming metastable energy barriers through Arrhenius-type relaxation processes. A rapid estimation can be made for our system, considering that the relaxation time of each crystallite or magnetic grain follows the Arrhenius law $\tau_m = \tau_0 \exp(K\ V/k_B T)$; taking the measuring time τ_m = 100 s (typical value for DC measurements), $\tau_0 = 10^{-10}$ s (τ_0 is the microscopic attempt time), and the anisotropy constant K as the effective value K_{eff}(24 K) = 2.7 x 10^5 J/m^3 (from the data shown in Figure 4b), gives a volume V corresponding to magnetic grains of diameter D_{Arrh} ~ 4 nm. This result is in good agreement with the grain size obtained by TEM, so it is possible that each crystallite acts as an activation or Barkhausen volume in the magnetization reversal process.

In order to have a further insight on this blocked contribution and its possible origin, we analyzed the T_B dependence on the applied magnetic field, for which ZFC-FC curves were measured at 50 mT, 100 mT and 200 mT (see inset of Figure 5b) and the corresponding blocking temperatures $T_B(H)$ were determined as the maxima of the $\partial[M_{ZFC}\text{-}M_{FC}]/\partial T$ corresponding curves. Considering that thermal activation processes originate in localized nuclei of the NWs [57], an analogy to particulate systems can be made.

It is known that for non-interacting magnetic particles, $T_B(H)$ is described by the simple analytical expression:

$$T_B(H) = \frac{K_{eff}V}{k_B \ln(\tau_m/\tau_0)}\left[1 - \frac{H}{H_A}\right]^{\alpha} \qquad (4)$$

where K_{eff} is the effective anisotropy constant, V is the particle volume, k_B is the Boltzmann's constant, H_A is the anisotropy field, τ_0 and τ_m have been previously defined and the exponent α is, in general close to 1.5.

The $T_B(H)$ experimental data of $Fe_{65}Pd_{35}$ NWs cannot be described by Eq. 4, probably because grain interactions cause deviations of the expected $T_B(H)$ trend for non-interacting systems [49, 50].

Devi et. al. [30] and Nunes et. al. [31] have developed a phenomenological model to describe $T_B(H)$ in particulate systems that assumes magnetic coupling between nanoparticles. The model is based on a simple modification of the random anisotropy model (RAM) that takes into account not an individual particle but rather a cluster of particles, and the dependence of the correlation length (L_H) with the magnetic field, defined as:

$$L_H = D_{av} + \sqrt{\frac{2A_{eff}}{M_S H + C}}, \qquad (5)$$

where D_{av} is the average diameter of the nanoparticles, A_{eff} describes an effective interaction intensity (which in the case of nanocrystalline alloys is the intergranular exchange constant A), and C is a constant introduced to eliminate the divergence of L_H when H goes to zero. According to this model, the nanoparticles volume is replaced by an effective volume ($\Lambda = \frac{\pi}{6}L_H^3$) and the anisotropy constant is averaged to an effective value K_{eff}. Substituting by Λ the volume of individual grains in Eq. 4, using L_H given by Eq. 5 and $H_A = 2K_{eff}/M_s$, the field dependence of the blocking temperature for coupled magnetic grains in terms of the structural parameters is [31]:

$$T_B = \frac{K_{eff}}{25k_B}\frac{\pi}{6}\left(D_{av} + \sqrt{\frac{2A_{eff}}{MsH + C}}\right)^3 \left[1 - \left(\frac{HM_S}{2K_{eff}}\right)\right]^{3/2} \qquad (6)$$

The $T_B(H)$ data obtained for our $Fe_{65}Pd_{35}$ NW array were fitted using Eq.(6) with the input parameters M_s= 1.474 x 10^6 A/m and K_{eff} (24 K) = 2.7 x 10^5 J/m^3 (from the data shown in Figure 4b), leaving D_{av} and A_{eff} as free parameters. The fit yields D_{av} = (3.3 ± 0.2) nm and A_{eff} = (2.2 ± 0.3) x 10^{-14} J/m and is shown in Figure 5b as a red solid line. It is clear from this figure that the interacting model provides a very good description of the T_B field dependence, which supports the hypothesis that the small grains in the NWs are the responsible for the blocked contribution.

The comparison between the D values obtained by different techniques is shown in Table 1, together with the parameters that were obtained from the fitting. The value of D_{av} suggests a magnetic diameter similar to

the grain size observed by TEM, to the crystallite size obtained by DRX using the Scherrer formula and to the estimated size from the Arrhenius law, confirming our hypothesis that the polycrystalline microstructure of the NWs is the responsible of the small activation volumes which are susceptible to thermal activation processes, even when shape anisotropy and magnetostatic/dipolar interactions are dominant in the NW array. These magnetic nanograins seem to be exchange-coupled up to second nearest-neighbors, since the correlation length at zero applied field L_0 is (7.5 ± 0.5) nm and might be the origin of the observed enhanced magnetic anisotropy in the array.

Table 1. Crystallite size D_{SCH}, particle size D_{TEM}, estimated size from the Arrhenius law D_{Arrh} and fitting parameters obtained by fitting experimental $T_B(H)$ data with the modified RAM model, Eq. 6.

			Fitting parameters of Eq. 6		
D_{SCH} [nm]	D_{TEM} [nm]	D_{Arrh} [nm]	D_{av} [nm]	L_0[nm]	A_{eff} [J/m]
6 ± 4	5 ± 1	4 ± 2	3.3 ± 0.2	7.5 ± 0.5	(2.2 ± 0.3) x10^{-14}

4. Conclusion

Bimetallic $Fe_{65}Pd_{35}$ NWs, (200 ± 20) nm in diameter and about (10 ± 1) μm long were successfully electrodeposited into the pores of an AAO template. As-deposited NWs are composed of the *fcc* and *bcc* phases of the Fe-Pd alloy. From the analysis of the $M(H)$ loops in PA and PE orientation at room temperature, the anisotropy field H_A = 0.33 T and the effective anisotropy constant at room temperature K_{eff} = 2.4 x 10^5 J/m^3 were obtained. The easy magnetization axis of the arrays is parallel to the NWs axis, as expected for a dominant contribution of shape effects; this is supported by the decreasing behavior of H_c with T, however this is less than the expected decrease if shape were the only source of anisotropy. Furthermore, the effective anisotropy constant, K_{eff}, has been also determined using the LATS in the temperature range from 10 K (2.8 x 10^5 J/m^3) up to 350 K (2.2 x 10^5 J/m^3).

Considering the polycrystalline microstructure of the NWs, an analogy with magnetic particulate systems was conceived, and the blocking temperature T_B dependence on the magnetic field H was analyzed using a modified RAM model. The results indicate that despite the overall behavior of the $Fe_{65}Pd_{35}$ NW array at room temperature is controlled by shape anisotropy and magnetostatic interactions between the NWs, a blocked magnetic contribution is present arising from the smaller grains in the NWs, which are coupled up to second nearest neighbors. Magnetic interactions among these nanograins are possibly responsible for the observed enhancement in the effective magnetic anisotropy of the array.

Acknowledgments

Overall support of Dr. Cristina Bran from ICMM/CSIC is acknowledged. P. G. B. acknowledges funding from SeCyT (Universidad Nacional de Córdoba), ANPCyT-FonCyT (Argentina) and CONICET (Argentina). M. V. acknowledges financial support from the Spanish Ministry of Innovation and Science under project PID2019-108075RB-C31/AEI/10.13039/501100011033 and the Regional Government of Madrid under project P2018/NMT-4321 NANOMAGCOST.

References

[1] S. Duan and R. Wang, "Bimetallic nanostructures with magnetic and noble metals and their physicochemical applications," *Prog. Nat. Sci. Mater. Int.*, vol. 23, no. 2, pp. 113–126, **2013**, doi: 10.1016/J.PNSC.2013.02.001.

[2] L. M. Sánchez and V. A. Álvarez, "Advances in magnetic noble metal/iron-based oxide hybrid nanoparticles as biomedical devices," *Bioengineering*, vol. 6, no. 3, **2019**, doi: 10.3390/bioengineering6030075.

[3] S. A. Morley, S. T. Riley, J. Porro, M. C. Rosamond, E. H. Linfield, J. E. Cunningham, S. Langridge and C. H. Marrows, "Effect of FePd alloy composition on the dynamics of artificial spin ice," *Sci. Rep.*, vol. 8, no. 1, pp. 4–11, **2018**, doi: 10.1038/s41598-018-23208-6.

[4] B. Martínez, A. Roig, X. Obradors, E. Molins, A. Rouanet, and C. Monty, "Magnetic properties of γ-Fe_2O_3 nanoparticles obtained by vaporization condensation in a solar furnace," *J. Appl. Phys.*, vol. 79, no. 5, pp. 2580–2586, **1996**, doi: 10.1063/1.361125.

[5] J. S. Riva, G. Pozo-López, A. M. Condó, L. M. Fabietti, and S. E. Urreta, "Low temperature ferromagnetism in Rh-rich Fe-Rh granular nanowires," *J. Alloys Compd.*, vol. 747, pp. 1008–1017, **2018**, doi: 10.1016/J.JALLCOM.2018.03.091.

[6] J. S. Riva, A. V. Juárez, S. E. Urreta, and L. M. Yudi, "Catalytic properties of FePd ferromagnetic nanowires at liquid/liquid interfaces," *Electrochim. Acta*, vol. 298, pp. 379–388, **2019**, doi: 10.1016/J.ELECTACTA.2018.12.069.

[7] A. Fernández-Pacheco, R. Streubel, O. Fruchart, R. Hertel, P. Fischer, and R. P. Cowburn, "Three-dimensional nanomagnetism," *Nat. Commun.*, vol. 8, no. 1, **2017**, doi: 10.1038/ncomms15756.

[8] P. Fischer, D. Sanz-Hernández, R. Streubel, and A. Fernández-Pacheco, "Launching a new dimension with 3D magnetic nanostructures," *APL Mater.*, vol. 8, no. 1, **2020**, doi: 10.1063/1.5134474.

[9] C. Bran, E. Berganza, J. A. Fernández-Roldán, E. M. Palmero, J. Meier, E. Calle, M. Jaafar, M. Foerster, L. Aballe, A. Fraile Rodríguez, R. Peréz del Real, A. Asenjo, O. Chubykalo-Fesenko and M. Vázquez, "Magnetization Ratchet in Cylindrical Nanowires," *ACS Nano*, vol. 12, no. 6, pp. 5932–5939, **2018**, doi:

10.1021/acsnano.8b02153.
[10] M. Vázquez, *Magnetic Nano- and Microwires: Design, Synthesis, Properties and Applications*, 2nd ed. United Kingdom: Woodhead Publishing, **2020**. [Online]. Available:https://www.elsevier.com/books/magnetic-nano-and-microwires/vazquez/978-0-08-102832-2
[11] N. Ahmad, J. Y. Chen, J. Iqbal, W. X. Wang, W. P. Zhou, and X. F. Han, "Temperature dependent magnetic properties of Co nanowires and nanotubes prepared by electrodeposition method," *J. Appl. Phys.*, vol. 109, no. 7, pp. 2011–2014, 2011, doi: 10.1063/1.3566077.
[12] M. Vázquez, "Cylindrical nanowire arrays: From advanced fabrication to static and microwave magnetic properties," *J. Magn. Magn. Mater.*, vol. 543, p. 168634, **2022**, doi: 10.1016/J.JMMM.2021.168634.
[13] Y. Zhang, M. Zhang, Z. Cai, M. Chen, and F. Cheng, "A novel electrochemical sensor for formaldehyde based on palladium nanowire arrays electrode in alkaline media," *Electrochim. Acta*, vol. 68, pp. 172–177, **2012**, doi: 10.1016/J.ELECTACTA.2012.02.050.
[14] A. Serrà, S. Grau, C. Gimbert-Suriñach, J. Sort, J. Nogués, and E. Vallés, "Magnetically-actuated mesoporous nanowires for enhanced heterogeneous catalysis," *Appl. Catal. B Environ.*, vol. 217, pp. 81–91, **2017**, doi: 10.1016/J.APCATB.2017.05.071.
[15] E. Herrera, M. S. Aprea, J. S. Riva, O. F. Silva, P. G. Bercoff, and A. Granados, "FePd nanowires modified with cyclodextrin. Characterization and catalytic properties evaluated by a model reduction reaction," *Appl. Surf. Sci.*, vol. 529, p. 147029, **2020**, doi: 10.1016/J.APSUSC.2020.147029.
[16] A. Nan, R. Turcu, C. Tudoran, M. Sofronie, and A. Chiriac, "Analysis of Functionalized Ferromagnetic Memory Alloys from the Perspective of Developing a Medical Vascular Implant," *Polymers*, vol. 14, no. 7. **2022**. doi: 10.3390/polym14071397.
[17] M. Cialone, F. Celegato, F. Scaglione, G. Barrera, D. Raj, M. Coïsson, P. Tiberto and P. Rizzi, "Nanoporous FePd alloy as multifunctional ferromagnetic SERS-active substrate," *Appl. Surf. Sci.*, vol. 543, p. 148759, **2021**, doi: 10.1016/j.apsusc.2020.148759.
[18] H. Hu, C. Yang, J. Chen, and G. Wu, "Magnetic properties of Fe0.95Pd0.05 nanowire arrays," *J. Magn. Magn. Mater.*, vol. 320, no. 18, pp. 2305–2309, 2008, doi: 10.1016/j.jmmm.2008.04.157.
[19] X. L. Fei, S. L. Tang, R. L. Wang, H. L. Su, and Y. W. Du, "Fabrication and magnetic properties of Fe-Pd nanowire arrays," *Solid State Commun.*, vol. 141, no. 1, pp. 25–28, 2007, doi: 10.1016/j.ssc.2006.09.042.
[20] R. D. James and M. Wuttig, "Magnetostriction of martensite," *Philos. Mag. A Phys. Condens. Matter, Struct. Defects Mech. Prop.*, vol. 77, no. 5, pp. 1273–1299, **1998**, doi: 10.1080/01418619808214252.
[21] Y. Ma, M. Zink, and S. G. Mayr, "Biocompatibility of single crystalline Fe_{70} Pd_{30} ferromagnetic shape memory films," *Appl. Phys. Lett.*, vol. 96, no. 21, pp. 2008–2011, **2010**, doi: 10.1063/1.3435260.
[22] K. Žužek Rožman, D. Pečko, S. Šturm, U. Maver, P. Nadrah, M. Bele, and S. Kobe,"Electrochemical synthesis and characterization of $Fe_{70}Pd_{30}$ nanotubes for drug-delivery applications," *Mater. Chem. Phys.*, vol. 133, no. 1, pp. 218–224, **2012**, doi: 10.1016/J.MATCHEMPHYS.2012.01.013.
[23] E. Herrera, J. Riva, S. Aprea, O. F. Silva, P. G. Bercoff, and A. M. Granados, "FePd nanowires modified with cyclodextrin as improved catalysts: effect of the alloy composition on colloidal stability and catalytic capacity," *Catal. Sci. Technol.*, vol. 12, pp. 2962–2971, **2022**, doi: 10.1039/d1cy02219a.
[24] K. J. Bryden and J. Y. Ying, "Electrodeposition synthesis and hydrogen absorption properties of nanostructured palladium-iron alloys," *Nanostructured Mater.*, vol. 9, no. 1–8, pp. 485–488, **1997**, doi: 10.1016/S0965-9773(97)00106-2.
[25] D. L. Hou, X. F. Nie, and H. L. Luo, "Magnetic anisotropy and coercivity of ultrafine iron particles," *J. Magn. Magn. Mater.*, vol. 188, no. 1–2, pp. 169–172, **1998**, doi: 10.1016/S0304-8853(98)00170-X.
[26] B. K. Chatterjee, C. K. Ghosh, and K. K. Chattopadhyay, "Temperature dependence of magnetization and anisotropy in uniaxial NiFe2O4 nanomagnets: Deviation from the Callen-Callen power law," *J. Appl. Phys.*, vol. 116, no. 15, **2014**, doi: 10.1063/1.4898089.
[27] L. Kumar, P. Kumar, S. K. Srivastava, and M. Kar, "Low temperature and high magnetic field dependence and magnetic properties of nanocrystalline cobalt ferrite," *J. Supercond. Nov. Magn.*, vol. 27, no. 7, pp. 1677–1681, **2014**, doi: 10.1007/s10948-014-2519-y.
[28] J. Wang, H. Duan, X. Lin, V. Aguilar, A. Mosqueda, and G. M. Zhao, "Temperature dependence of magnetic anisotropy constant in iron chalcogenide Fe3Se4: Excellent agreement with theories," *J. Appl. Phys.*, vol. 112, no. 10, 2012, doi: 10.1063/1.4759352.
[29] M. Vázquez, W. Fernengel, and H. Kronmüller, "Approach to magnetic saturation in rapidly quenched amorphous alloys," *Phys. Status Solidi*, vol. 115, no. 2, pp. 547–553, **1989**, doi: 10.1002/pssa.2211150223.
[30] E. C. Devi and I. Soibam, "Law of Approach to Saturation in Mn–Zn Ferrite Nanoparticles," *J. Supercond. Nov. Magn.*, vol. 32, no. 5, pp. 1293–1298, **2019**, doi: 10.1007/s10948-018-4823-4.
[31] W. C. Nunes, L. M. Socolovsky, J. C. Denardin, F. Cebollada, A. L. Brandl, and M. Knobel, "Role of magnetic interparticle coupling on the field dependence of the superparamagnetic relaxation time," *Phys. Rev. B - Condens. Matter Mater. Phys.*, vol. 72, no. 21, **2005**, doi: 10.1103/PhysRevB.72.212413.
[32] K. H. J. Buschow, P. G. Van Engen, and R. Jongebreur, "Magneto-optical properties of metallic ferromagnetic materials," *J. Magn. Magn. Mater.* vol. 38. no. 1, pp. 1–22. **1983**. https://doi.org/10.1016/0304-8853(83)90097-5
[33] Z. Wang, W. Wu, X. Bian, and Y. Wu, "Synthesis and characterization of amorphous Al_2O_3 and γ-Al_2O_3 by spray pyrolysis," *Green Process. Synth.*, vol. 5, no. 3, pp. 305–310, **2016**, doi: 10.1515/gps-2015-0128.
[34] K. Z. Rožman, D. Pečko, S. Trafela, Z. Samardzija, M. Spreitzer, Z. Jaglicic, P Nadrah, M. Zorko, M. Bele, T. Tisler, A. Pintar, S. Sturm and N. Kostevsek, "Austenite-martensite transformation in electrodeposited $Fe_{70}Pd_{30}$ NWs: A step towards making bio-nano-actuators tested on in vivo systems," *Smart Mater. Struct.*, vol. 27, no. 3, **2018**, doi: 10.1088/1361-665X/aaacb0.
[35] D. Vokoun, T. Goryczka, and C. T. Hu, "Thermomechanical and magnetic properties of the as-spun Fe–Pd SMA ribbons," *J. Alloys Compd.*, vol. 372, no. 1–2, pp. 165–168, **2004**, doi: 10.1016/J.JALLCOM.2003.09.154.
[36] D. Pečko, S. Šturm, S. Kobe and K. Žužek Rožman, "Potentiostatically Electrodeposited Hard-Magnetic Fe–Pd-Based Nanowires," *IEEE Trans. Magn.*, vol. 51, no. 7, **2015**. doi:10.1109/TMAG.2015.2392083.
[37] K. Ž. Rožman, D. Pečko, L. Suhodolčan, P. J. McGuiness, and S. Kobe, "Electrochemical syntheses of soft and hard magnetic $Fe_{50}Pd_{50}$-based nanotubes and their magnetic characterization," *J. Alloys Compd.*, vol. 509, no. 2, pp. 551–555, **2011**, doi: 10.1016/j.jallcom.2010.09.108.
[38] D. Pečko, K. Ž. Rožman, N. Kostevšek, M. Shahid Arshad, B. Markoli, Zoran Samardžija and S. Kobe, "Electrodeposited hard-magnetic $Fe_{50}Pd_{50}$ nanowires from an ammonium-citrate-based bath," *J. Alloys Compd.*, vol. 605, pp. 71–79, **2014**, doi: 10.1016/j.jallcom.2014.03.156.
[39] L. Piraux, "Magnetic nanowires," *Appl. Sci.*, vol. 10, no. 5, p. 1832, **2020**, doi: 10.3390/app10051832.
[40] C. Bran, E. M. Palmero, Zi-An Li, R. Peréz del Real, M.

Spasova, M. Farle and M. Vázquez, "Correlation between structure and magnetic properties in Co_xFe_{100-x} nanowires: The roles of composition and wire diameter," *J. Phys. D. Appl. Phys.*, vol. 48, no. 14, **2015**, doi: 10.1088/0022-3727/48/14/145304.
[41] M. S. Salem, P. Sergelius, R. Zierold, J. M. Montero Moreno, D. Görlitz, and K. Nielsch, "Magnetic characterization of nickel-rich NiFe nanowires grown by pulsed electrodeposition," *J. Mater. Chem.*, vol. 22, no. 17, pp. 8549–8557, **2012**, doi: 10.1039/c2jm16339j.
[42] H. Shima, K. Oikawa, A. Fujita, K. Fukamichi, K. Ishida, and A. Sakuma, "Lattice axial ratio and large uniaxial magnetocrystalline anisotropy in L10-type FePd single crystals prepared under compressive stress," *Phys. Rev. B - Condens. Matter Mater. Phys.*, vol. 70, no. 22, **2004**, doi: 10.1103/PhysRevB.70.224408.
[43] A. Korolev, N. Vlasova, O. Golovina, S. Okatov, J. Barker, B. G.reenberg, O. Klementjeva, A. Volkov and O. N. Mryasoc, "Temperature dependence of magnetic anisotropy for single domain L10 FePd crystal and role of the ordering defects," *2015 IEEE Int. Magn. Conf. INTERMAG 2015*, vol. 2, no. 0, p. AD-06, **2015**, doi: 10.1109/INTMAG.2015.7156517.
[44] J. Jorritsma and J. A. Mydosh, "Temperature-dependent magnetic anisotropy in Ni nanowires," *J. Appl. Phys.*, vol. 84, no. 2, pp. 901–906, 1998, doi: 10.1063/1.368154.
[45] B. D. Cullity, Introduction to Magnetic Materials. Addison-Weseley Publishing Co., Reading, 1972.
[46] C. Rotarescu, R. Moreno, J. A. Fernández-Roldán, D. G. Trabada, N. M. Nemes, T. Fehér, C. Bran, M. Vázquez, H. Chiriac, N. Lupu, T. A. Óvári, and O. Chubykalo-Fesenko, "Effective anisotropies in magnetic nanowires using the torque method," *J. Magn. Magn. Mater.*, vol. 443, pp. 378–384, 2017, doi: 10.1016/j.jmmm.2017.07.059.
[47] V. Raposo, M. Zazo, A. G. Flores, J. García, V. Vega, J. Iñiguez, and V. M. Prida, "Ferromagnetic resonance in low interacting permalloy nanowire arrays", *J. Appl. Phys.*, vol. 119, no. 14, 2016, doi: 10.1063/1.4945762.
[48] F. Meneses, S. E. Urreta, J. Escrig, and P. G. Bercoff, "Temperature dependence of the effective anisotropy in Ni nanowire arrays," *Curr. Appl. Phys.*, vol. 18, no. 11, pp. 1240–1247, 2018, doi: 10.1016/j.cap.2018.06.014.
[49] V. Recarte, C. Gómez-Polo, V. Sánchez-Alárcos, and J. I. Pérez-Landazábal, "Magnetic study of the martensitic transformation in a Fe–Pd alloy," *J. Magn. Magn. Mater.*, vol. 316, no. 2, pp. e614–e617, **2007**, doi: 10.1016/J.JMMM.2007.03.044.
[50] P. M. Paulus, F. Luis, M. Kröll, G. Schmid, and L. J. De Jongh, "Low-temperature study of the magnetization reversal and magnetic anisotropy of Fe, Ni, and Co nanowires," *J. Magn. Magn. Mater.*, vol. 224, no. 2, pp. 180–196, **2001**, doi: 10.1016/S0304-8853(00)00711-3.
[51] J. Cui, T. W. Shield, and R. D. James, "Phase transformation and magnetic anisotropy of an iron-palladium ferromagnetic shape-memory alloy," *Acta Mater.*, vol. 52, no. 1, pp. 35–47, **2004**, doi: 10.1016/j.actamat.2003.08.024.
[52] C. A. Ramos, E. V. Brigneti, and M. Vazquez, "Self-organized nanowires: Evidence of dipolar interactions from ferromagnetic resonance measurements," *Phys. B Condens. Matter*, vol. 354, no. 1-4 SPEC. ISS., pp. 195–197, 2004, doi: 10.1016/j.physb.2004.09.047.
[53] L. Forzani, A. M. Gennaro, R. R. Koropecki, and C. A. Ramos, "Sensing anisotropic stresses with ferromagnetic nanowires," *Appl. Phys. Lett.*, vol. 116, no. 1, 2020, doi: 10.1063/1.5132539.
[54] E. B. Peixoto, M. H. Carvalho, J. G. S. Duque, D. Muraca, Y. T. Xing, and W. C. Nunes, "Size distribution and interaction effects on dispersed Fe30Ni70 nanoalloy synthesized by thermal decomposition," *J. Magn. Magn. Mater.*, vol. 518, p. 167399, **2021**, doi: 10.1016/J.JMMM.2020.167399.
[55] J. P. Wang, D.-H. Han, H.-L. Luo, Q.-X. Lu, and Y.-W. Sun, "Study on the coercivity of granular solid iron," *Appl. Phys. A.* vol. 61, no. 4, pp. 401–313, **1995**. doi: 10.1007/s003390050220.
[56] Helmut Kronmüller and M. Fähnle, *Micromagnetism and the Microstructure of Ferromagnetic Solids*. Cambridge University Press, **2003**. [Online]. Available: http://www.cambridge.org/asia/catalogue/catalogue.asp?isbn=9780521331357&ss=exc
[57] R. Skomski, H. Zeng, and D. J. Sellmyer, "Incoherent magnetization reversal in nanowires," *J. Magn. Magn. Mater.*, vol. 249, no. 1–2, pp. 175–180, **2002**, doi: 10.1016/S0304-8853(02)00527-9.